Integral Equation Solvers and Their Applications in the Optical Regime

E. Simsek* Q. H. Liu†

Abstract — **This paper presents integral equation solvers to calculate the electromagnetic field scattered from objects embedded in a multilayered medium. First, the electric field surface integral equation (SIE) is solved using method of moments for homogeneous objects. Then, this SIE is used as an exact radiation boundary condition to truncate the computational domain in the finite-element method (FEM) to form a hybrid SIE-FEM, which is applicable to arbitrary inhomogeneous objects embedded in a multilayered medium. The efficiency and accuracy of the developed methods have been demonstrated with numerical experiments both in microwave and optical regimes.**

1 INTRODUCTION

Recent developments in nano-fabrication, which allows metals to be structured and characterized on the nanometer scale, inspire a wide spectrum of engineers and scientists to develop new types of photonic devices, sensors, and optical antennas. In this direction, the fundamental understanding and control over the properties of surface plasmons (SPs), which are simply electromagnetic waves that propagate along the surface of a conductor, is crucial for the current and future SP applications such as surface or tip enhanced Raman scattering and nonlinear frequency generation. In these applications, researchers aim to tune up the properties of SPs and their interaction with light depending on the problem of interest by changing the shape, size, and material composition of the nanoparticles. Frequently, researchers support their experimental observations with the simulation results obtained using time-domain methods. However, it is very well known that time-domain methods might not be able to provide very accurate results for high-Q structures. One way to overcome this problem is using a frequency domain method.

This work deals first with developing a surface integral equation (SIE) frequency domain solver based on Method of Moments to calculate electromagnetic (EM) scattered field from homogeneous objects embedded in a layered medium. Then, this SIE solver is adopted as a radiation boundary, where the volume enclosed by that boundary is meshed and solved with a finite element method (FEM) frequency domain solver. For the implementation of 3D radiation boundary condition, an artificial boundary, Γ, is applied to truncate the arbitrarily 3D shaped inhomogenous scatterer(s) from the layered medium. The FEM is applied in the interior region to calculate the field, while the method of moments is applied on the outer boundary, Γ, to relate the field and the induced current. Due to the form of the chosen basis functions and meshing, the fields and currents on the boundary for the FEM are obtained from the solution of the final matrix equation without using any interpolation. This algorithm stores the sparse and symmetric FEM matrix by using a row-indexed scheme to reach its the non-zero elements quickly for the sake of computational efficiency; and it solves for the coupled SIE-FEM matrix by using the biconjugate-gradient method. In addition, the CPU time for the evaluation of layered medium Green's functions is reduced by a simple interpolation technique.

These numerical algorithms can handle dispersive materials in the optical regime, which is crucial for the design and analysis of plasmonic structures and optical antennas. The accuracy of the implementation is validated by several numerical examples demonstrating the optical near field enhancement and surface plasmon resonance of metal nanoparticles periodically aligned in a multilayered medium.

2 FORMULATION

In this section, we briefly describe the theory behind MoM, FEM, and hybrid SIE-FEM solvers.

2.1 Method of Moments

Assume that there is an arbitrarily shaped homogeneous object with surface S, electrical permittivity ϵ_s, and permeability μ_s. The object is located in a multilayered background. Layer-i is described by its own permittivity, permeability, and height (ϵ_i, μ_s, and h_i), where $i = 1, 2, \cdots, N_L$ and N_L is the number of layers. In order to calculate the EM field

*Department of Electrical and Electronics Engineering, Bahcesehir University, Istanbul, TURKEY. e-mail: ergun.simsek@bahcesehir.edu.tr, tel: +90 212 3810583, fax: +90 212 3810550.

†Department of Electrical and Computer Engineering, Duke University, Durham, NC, USA. e-mail: qhliu@ee.duke.edu, tel: +1 (919) 6605440, fax: +1 (919) 6605293.

978-1-4244-3386-5/09/$25.00 ©2009 IEEE

scattered from an object, one can solve for the electric field integral equations (EFIE) for the exterior and interior problems. The former can be written as follows

$$\begin{aligned}\mathbf{E} &= -j\omega\mu_i\langle\bar{\mathbf{K}}^J;\mathbf{J}\rangle \\ &+\tfrac{1}{j\omega\epsilon_i}\nabla\langle G_\Phi^{EJ},\nabla'\cdot\mathbf{J}\rangle+\langle\bar{\mathbf{G}}^{EM};\mathbf{M}\rangle\end{aligned} \quad (1)$$

where $\mathbf{J}$ and $\mathbf{M}$ are induced electric and magnetic currents, respectively, due to incident fields; ω is the angular frequency; $\bar{\mathbf{K}}^J$, G_Φ^{EJ}, $\bar{\mathbf{G}}^{EM}$ are different types of layered medium Green's functions [1]. For the numerical solution, the unknown currents, $\mathbf{J}$ and $\mathbf{M}$, are expanded in terms of the basis functions, $\mathbf{f}_n$ and $\mathbf{b}_n$, as

$$\begin{aligned}\mathbf{J}(\mathbf{r}) &= \textstyle\sum_{n=1}^{N_b} j_n\mathbf{f}_n(\mathbf{r}), \\ \mathbf{M}(\mathbf{r}) &= \textstyle\sum_{n=1}^{N_b} m_n\mathbf{b}_n(\mathbf{r}),\end{aligned} \quad (2)$$

where N_b is the number of interior edges on the surface of the object, j_n and m_n are the unknown coefficients for electric and magnetic current densities, respectively. When we apply the Galerkin type MoM, with the same type of functions for the testing $\mathbf{f}_m$ and $\mathbf{b}_m$, we obtain

$$S_m = \sum_{n=1}^{N_b} j_n\left[Z_{mn}^{(1)}+Z_{mn}^{(2)}\right]+\sum_{n=1}^{N_s} m_n Z_{mn}^{(3)} \quad (3)$$

where

$$S_m = \int_s \mathbf{f}_m\cdot E^{inc}ds, \quad (4)$$

$$Z_{mn}^{(1)} = jk_i\eta_i\int_s\int_{s'}\mathbf{f}_m\cdot\mathbf{K}^J\mathbf{f}_n ds'ds, \quad (5)$$

$$Z_{mn}^{(2)} = \frac{j\eta_i}{k_i}\int_s\int_{s'}\nabla\cdot\mathbf{f}_m\cdot G_\Phi^{EJ}\nabla'\cdot\mathbf{f}_n ds'ds, \quad (6)$$

$$\begin{aligned}Z_{mn}^{(3)} &= P.V.\textstyle\int_s\int_{s'}\mathbf{f}_m\cdot\nabla'\mathbf{G}^{EM}\times\mathbf{f}_n ds'ds \\ &-\tfrac{1}{2}\textstyle\int_s\mathbf{f}_m\cdot\mathbf{f}_n ds,\end{aligned} \quad (7)$$

where k_i and η_i wavenumber and intrinsic impedance of layer-i, respectively. EFIE for the interior problem is not provided for the sake of brevity.

The surface of the object is modeled using planar triangular patches and RWG (Rao, Wilton, Glisson) basis functions [2] are used to approximate the surface currents. For the numerical integration, Gaussian quadrature rules are followed and Duffy transformation is used for the self interaction terms. In order to reduce the CPU time for the evaluation of layered medium Green's functions, a simple interpolation technique is implemented.

2.2 Finite Element Method

Assume that a finite domain is discretized with tetrahedral elements and volume basis functions $\mathbf{\Phi}_n(\mathbf{r})$ to expand the unknown electric field along the whole volume. The numbers of inner and boundary edges are N_i and N_b, respectively, where $N = N_i + N_b$. Then, we can expand the unknown electric field and current as

$$\begin{aligned}\mathbf{E} = &\textstyle\sum_{n=1}^{N} E_n\mathbf{\Phi}_n(\mathbf{r}) \\ &= \textstyle\sum_{n=1}^{N_i} E_n^i\mathbf{\Phi}_n(\mathbf{r})+\sum_{n=1}^{N_b} E_n^b\mathbf{\Phi}_n(\mathbf{r}),\end{aligned} \quad (8)$$

$$\hat{\mathbf{n}}\times\mathbf{H} = \sum_{n=1}^{N_b} j_n\mathbf{f}_n(\mathbf{r}) \quad (9)$$

Then, the weak form volume electric field integral equation can be written as

$$[\mathbf{A}'+\mathbf{B}']\mathbf{E}+\mathbf{G}\mathbf{J} = \mathbf{S}^{\mathbf{i}} \quad (10)$$

where E_n, J_n are unknown coefficients, S_i are source and $\mathbf{A}', \mathbf{B}', \mathbf{G}$ are stiffness matrices defined as,

$$\begin{aligned}S_i &= -jk_0\eta_0\int_v\mathbf{\Phi}_i(\mathbf{r})\cdot\mathbf{S}dv \\ A'_{i,n} &= \int_v(\mu_r^{-1}\nabla\times\mathbf{\Phi}_n(\mathbf{r}))\cdot(\nabla\times\mathbf{\Phi}_i(\mathbf{r}))dv \\ B'_{i,n} &= -\bar{\epsilon}_r k_0^2\int_v\mathbf{\Phi}_n(\mathbf{r})\cdot\mathbf{\Phi}_i(\mathbf{r})dv \\ G_{i,n} &= jw\mu_0\oint_s\mathbf{f}_n(\mathbf{r})\times\mathbf{\Phi}_i(\mathbf{r})ds\end{aligned} \quad (11)$$

Furthermore, the matrix form can be written as,

$$\mathbf{A}\mathbf{E}^{\mathbf{i}}+\mathbf{B}\mathbf{E}^{\mathbf{b}} = \mathbf{S}^{\mathbf{i}} \quad (12)$$

$$\mathbf{B}^{\mathbf{T}}\mathbf{E}^{\mathbf{i}}+\mathbf{C}\mathbf{E}^{\mathbf{b}}+\mathbf{G}\mathbf{J} = \mathbf{0} \quad (13)$$

where matrices $\mathbf{A}, \mathbf{B}, \mathbf{C}$ are sub-matrices of the stiffness matrix $\{\mathbf{A}'+\mathbf{B}'\}$.

2.3 Coupling FEM and MoM Matrices

By using $\mathbf{M}(\mathbf{r}) = -\hat{\mathbf{n}}\times\mathbf{E}|_s$, we can couple FEM and MoM equations as

$$\begin{bmatrix}\mathbf{A} & \mathbf{B} & \\ \mathbf{B}^T & \mathbf{C} & \mathbf{G} \\ & \mathbf{Z^{(3)}} & \mathbf{D}\end{bmatrix}\begin{bmatrix}\mathbf{E^i}\\ \mathbf{E^b}\\ \mathbf{J}\end{bmatrix} = \begin{bmatrix}\mathbf{S^i}\\ \mathbf{0}\\ \mathbf{S^e}\end{bmatrix}, \quad (14)$$

where $\mathbf{D} = \mathbf{Z^{(1)}}+\mathbf{Z^{(2)}}$. However, it should be noted that the above formulation is only valid if the FEM mesh matches the MoM mesh on the boundary. In order to couple arbitrary meshes, some additional interpolation functions are required.

The matrix Eq. 14 is a straight-forward solution but not the most efficient one. In order to take

advantage of having a sparse and symmetric FEM matrix, the matrix equations 3 and 14 are reformulated as follows

$$\mathbf{D}\,\mathbf{J} + \mathbf{F}\,\mathbf{E^b} = \mathbf{S^e}, \tag{15}$$

and

$$\begin{bmatrix} \mathbf{A} & \mathbf{B} \\ \mathbf{B}^T & \mathbf{C} \end{bmatrix} \begin{bmatrix} \mathbf{E}^i \\ \mathbf{E}^b \end{bmatrix} = \begin{bmatrix} 0 & 0 \\ 0 & \mathbf{G} \end{bmatrix} \begin{bmatrix} 0 \\ \mathbf{J} \end{bmatrix} + \begin{bmatrix} \mathbf{S}^i \\ 0 \end{bmatrix}, \tag{16}$$

respectively, where $\mathbf{F} = \mathbf{Z^{(3)}}$. In Eq. 15, we can leave the electric current alone on the left hand side and substitute it into Eq. 16

$$\begin{bmatrix} \mathbf{A} & \mathbf{B} \\ \mathbf{B}^T & \mathbf{C} - \mathbf{G}\mathbf{D^{-1}}\mathbf{F} \end{bmatrix} \begin{bmatrix} \mathbf{E}^i \\ \mathbf{E}^b \end{bmatrix} = \begin{bmatrix} \mathbf{S}^i \\ \mathbf{D^{-1}}\mathbf{S^e} \end{bmatrix}, \tag{17}$$

which is more compact than Eq. 14.

Since the FEM matrix is symmetric, the Hermitian of this matrix is simply its complex conjugate. Moreover, the FEM matrix is sparse. By using a row-indexed scheme [3], we can easily and efficiently reach the non-zero elements of the FEM matrix, which is a very important property for the solvers constructed based on the biconjugate-gradient (BCG) method . As a result, it is more efficient to store the FEM and MoM matrices seperately as follows,

$$\left(\begin{bmatrix} \mathbf{A} & \mathbf{B} \\ \mathbf{B}^T & \mathbf{C} \end{bmatrix} + \begin{bmatrix} 0 & 0 \\ 0 & -\mathbf{G}\mathbf{D^{-1}}\mathbf{F} \end{bmatrix} \right) \times \begin{bmatrix} \mathbf{E}^i \\ \mathbf{E}^b \end{bmatrix} = \begin{bmatrix} \mathbf{S}^i \\ \mathbf{D^{-1}}\mathbf{S^e} \end{bmatrix}. \tag{18}$$

It should be noted that once we calculate the layered-medium Greens function for the radiation boundary, we can use it several times for any type of object inside that boundary.

3 NUMERICAL RESULTS

A systematic study of metal nanoparticles (NPs) is conducted to understand the effect of the number of NPs on the optical cross section. The number of of gold nanorods is increased from 1 to 16 step by step. The gold nanorods, which are 50 nm height, 60 nm wide and 140 nm long, are aligned on top of a thick silica substrate. Figure 1 depicts a single nanorod. The experimental values for the optical constants of gold are used [4] rather than the Drude model, to avoid the concerns regarding the selection of the appropriate plasmon and relaxation frequency values.

The background is assumed to be a 2-layer medium, where the air-silica interface occurs at $z = 0$ nm. The refractive indices of air and silica

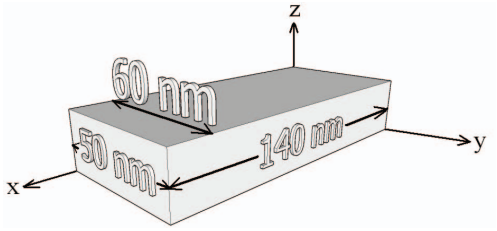

Figure 1: 50 nm height, 60 nm wide and 140 nm long nanorod.

are assumed to be 1 and 1.53, respectively. Incident field is a plane wave traveling along the $+z$ direction and the electric field is polarized in the $+x$ direction.

The average power ($E_y * H_x/2$) is calculated at $z = 200$ nm over a range of wavelengths (frequencies) using MoM/FEM and WNT (a pseudo-spectral domain solver, [5]). For both solvers, the sampling density is 20 points per wavelength. Figure 2 shows the good match between MoM/FEM and WNT solutions for 3 nanorods, which are 180 nm apart from each other along the y-axis. Both solutions state that the minimum transmission occurs around $\lambda = 718$ nm.

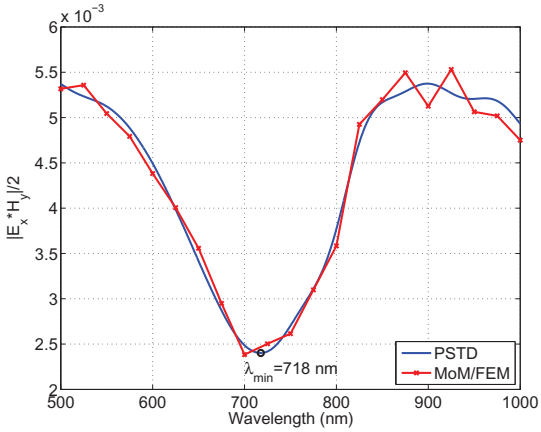

Figure 2: The average power on top of 3 nanorods over a range of wavelengths.

The same procedure is followed for different N values, where N is number of nanorods. For each setup, the inter particle spacing along the y axis is 180 nm. Figure 3 shows the wavelength values, which give the minimum transmission, for $N = 1, 2, \cdots, 16$. Clearly, as N increases, the resonance wavelengths decrease. More importantly, the slope of this function goes to zero which means that

the longitudinal surface plasmon resonance mode of an optical waveguide -that consists of 50 nm height, 60 nm wide and 140 nm long gold nanorods fabricated on a silica slide- should be around 690 nm.

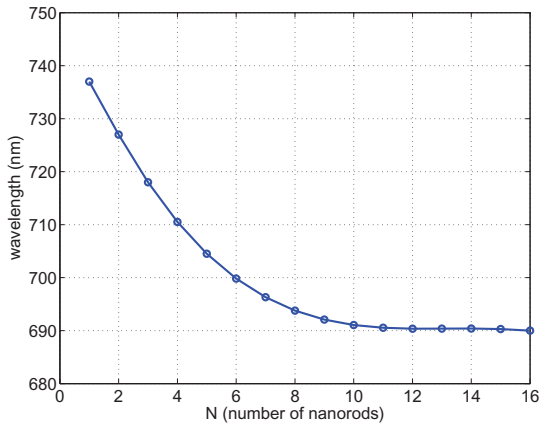

Figure 3: Number of nanorods vs. wavelength value which gives the minimum transmission.

4 CONCLUSION

Method of moments and finite element methods are implemented in numerically efficient integral equation solvers to calculate the electromagnetic field scattered from objects embedded in a multilayered medium. MoM and hybrid MoM/FEM solvers can deal with homogeneous and inhomogeneous scatterers, respectively, embedded in a multilayered medium. The use of SIE as a radiation boundary and layered medium Green's functions create a substantial saving in terms of memory and CPU time requirements. Since both solvers can work with complex permittivity and permeability, they serve as excellent tools for both microwave and optical region problems.

References

[1] E. Simsek, Q. H. Liu, and B. Wei, "Singularity subtraction for evaluation of Green's functions for multilayer media," *IEEE Trans. Microwave Theo. and Tech.*, vol. 54, no. 1, pp. 216-225, Jan. 2006.

[2] S. Rao, D. Wilton, A. Glisson, "Electromagnetic scattering by surfaces of arbitrary shape," *IEEE Trans. Antennas Propag.,* vol. 30, no. 3, pp. 409-418, May 1982.

[3] W. H. Press, S. A. Teukolsky, W. T. Vettering, and B. P. Flannery, *Numerical Recipes in C: The Art of Scientific Computing,* 2nd edition, New York: Cambridge University Press, 1992.

[4] D. Rakic, A. B. Djurisic, J. M. Elazar and M. L. Majewski, "Optical properties of metallic films for vertical-cavity optoelectronic devices," *Appl. Opt.*, vol. 37, pp. 5271-5283, 1998.

[5] PSTD software is WNT from Wave Computation Technologies, Durham, NC.